Supplemental Material — An Antisymmetric Berry Frictional Force At Equilibrium in the Presence of Spin-Orbit Coupling

Hung-Hsuan Teh
Department of Chemistry, University of Pennsylvania, Philadelphia, Pennsylvania 19104, USA

Wenjie Dou
School of Science, Westlake University, Hangzhou, Zhejiang 310024, China
Institute of Natural Sciences, Westlake Institute for Advanced Study, Hangzhou, Zhejiang 310024, China

Joseph E. Subotnik
Department of Chemistry, University of Pennsylvania, Philadelphia, Pennsylvania 19104, USA

In this SM, we provide a host of details as relevant to the main findings of the letter. In sections A-D, we both review and prove several properties of the friction tensor based on the quantum-classical Liouville equation. For instance (from Eq. (A1) below), it follows that $\gamma^*_{\mu\nu} = \gamma_{\mu\nu}$, so that the friction tensor is real-valued. Beyond this obvious statement, in Sec. A, we show that the friction tensor can be dramatically simplified in the absence of electron-electron interactions (leading to Eq. (2) in the main text of the letter). In Sec. B, we prove that the friction tensor is positive definite at equilibrium (with or without interactions). In Sec. C, we prove that the fluctuation-dissipation theorem holds (though we note that a previously reported proof was incorrect). In Sec. D, we prove that, for a real-valued Hamiltonian, the friction tensor is purely symmetric. In Sec. E, we provide a schematic picture of our molecular junction model. Armed with these facts, in section F of this SM, we derive Eqs. (3)-(5) of the main text of the letter. In sections G-I, we analyze friction in three different scenarios: G) the presence of a conical intersection, H) a changing temperature, and I) a variable coupling to the environment. In Sec. J, we apply our findings to a realistic molecule, diphenylmethane, between two gold atoms. We show that, for a realistic set of parameters, the antisymmetric friction tensor can be large — even for small spin-orbit couplings.

A. THE NON-INTERACTING FRICTION TENSOR UNDER THE CONDON APPROXIMATION

In Ref. 2, based on the quantum-classical Liouville equation (QCLE) and appropriate usages of the adiabatic theorem, a universal Fokker-Planck equation for a real-valued or complex-valued Hamiltonian was derived, either at equilibrium or in a nonequilibrium steady state with a Markovian[19–21, 49] electronic friction tensor of the form:

$$\gamma_{\mu\nu} = -\int_0^\infty dt\, \mathrm{Tr}\Big\{\partial_\mu \hat{H} e^{-i\hat{H}t} \partial_\nu \hat{\rho}_{\mathrm{ss}} e^{i\hat{H}t}\Big\}. \tag{A1}$$

Here $\hat{H}$ is the electronic Hamiltonian and $\hat{\rho}_{\mathrm{ss}}(\mathbf{R})$ is the steady-state density matrix at each nuclear position $\mathbf{R}$, i.e. $\partial_t \hat{\rho}_{\mathrm{ss}}(\mathbf{R}) = -i[\hat{H}(\mathbf{R}), \hat{\rho}_{\mathrm{ss}}(\mathbf{R})] = 0$. In Eq. (A1), the partial derivatives with respect to the nuclear coordinates μ, ν (i.e. ∂_μ, ∂_ν) operate only on the operator directly to the right, and this convention will be used throughout the letter below. The trace is taken over all the electronic degrees of freedom.

Equation (A1) can be further simplified when a general non-interacting Hamiltonian, $\hat{H} = \sum_{pq} \mathcal{H}_{pq} \hat{d}^\dagger_p \hat{d}_q + U(\mathbf{R})$ ($\hat{d}^\dagger_p/\hat{d}_p$ creates/annihilates an electron in orbital p, and $U(\mathbf{R})$ is a purely nuclear potential energy), is considered. The result is:

$$\gamma_{\mu\nu} = -\frac{1}{2\pi}\int_{-\infty}^{\infty} d\epsilon\, \mathrm{Tr}\big\{\partial_\mu \mathcal{H} \mathcal{G}^{\mathrm{R}} \partial_\nu \sigma_{\mathrm{ss}} \mathcal{G}^{\mathrm{A}}\big\}, \tag{A2}$$

where $\mathcal{G}^{\mathrm{R/A}} = (\epsilon - \mathcal{H} \pm i\eta)^{-1}$ are retarded/advanced Green's functions of the electrons, and $(\sigma_{\mathrm{ss}})_{pq} = \mathrm{Tr}\Big\{\hat{\rho}_{\mathrm{ss}} \hat{d}^\dagger_p \hat{d}_q\Big\}$ is the steady-state density matrix. In general, σ_{ss} is a complicated function of $\hat{H}$ so that the analytic derivative of the steady-state distribution (e.g. a Boltzmann distribution which depends on $\mathbf{R}$) is hard to calculate. Nevertheless, from this expression, one can show that $\gamma^{\mathrm{A}}_{\mu\nu}$ vanishes when $\hat{H}$ is real-valued and the system is in equilibrium; see SM D for a proof. In practice, we will use a nonequilibrium Green's function technique to treat σ_{ss}. Notice that σ_{ss} can be expressed in terms of the lesser Green's function in the frequency domain,

$$(\sigma_{\mathrm{ss}})_{pq} = -i\mathcal{G}^<_{pq}(t,t) = -i\int \frac{d\epsilon'}{2\pi} \mathcal{G}^<_{pq}(\epsilon'),$$

where the lesser Green's function $\mathcal{G}^{<}_{pq}(t_1,t_2) = i\mathrm{Tr}\Big\{\hat{\rho}_{\mathrm{ss}}\hat{d}^{\dagger}_p(t_2)\hat{d}_q(t_1)\Big\}$ is defined as usual. Since σ_{ss} applies at steady state, $\mathcal{G}^{<}(\epsilon)$ can be calculated by the Keldysh equation[43],

$$\mathcal{G}^{<} = \mathcal{G}^{\mathrm{R}}\Pi^{<}\mathcal{G}^{\mathrm{A}},$$

where $\Pi^{<}$ is the lesser self energy of the electrons. Here we artificially imagine very weakly embedding the total electronic Hamiltonian $\hat{H}$ in some fictitious surrounding so that $\Pi^{<}$ can be evaluated. Because, the interaction between $\hat{H}$ and the surrounding is taken as infinitesimally small, all properties we derive will not be affected by the introduction of an artificial surrounding. In general, $\mathcal{G}^{\mathrm{R,A}}$ and $\Pi^{<}$ can all possibly depend on $\mathbf{R}$. However, we further assume that $\Pi^{<}$ is independent of $\mathbf{R}$ so that $\gamma_{\mu\nu}$ can be substantially simplified. This assumption can be realized by imaging that the total electronic Hamiltonian $\hat{H}$ is composed of two parts: one that depends on $\mathbf{R}$ and the other that does not depend on $\mathbf{R}$, and only the later weakly couples to the surrounding. According to Ref. 42, using the assumptions above, one can transform Eq. (A2) into the following expression,

$$\gamma_{\mu\nu} = \int_{-\infty}^{\infty}\frac{d\epsilon}{2\pi}\mathrm{Tr}\big\{\partial_\mu\mathcal{H}\partial_\epsilon\mathcal{G}^{\mathrm{R}}\partial_\nu\mathcal{H}\mathcal{G}^{<}\big\} + \mathrm{H.c.}, \tag{A3}$$

Note that the potential $U(\mathbf{R})$ does not contribute to the friction tensor.

Finally, if we make the Condon approximation and assume that the coupling between the system and the bath $V_{m,k\alpha}$ is independent of the nuclear coordinate $\mathbf{R}$, the friction tensor in Eq. (A3) becomes Eq. (2) in the main text[42].

B. POSITIVE DEFINITENESS OF THE ELECTRONIC FRICTION TENSOR

In this section, we prove that both the electronic friction tensor $\gamma_{\mu\nu}$ and its symmetric part $\gamma^{\mathrm{S}}_{\mu\nu}$ are positive definite when the system is in equilibrium. That is, $\sum_{\mu\nu}X_\mu\gamma_{\mu\nu}X_\nu > 0$ for arbitrary real vectors $\mathbf{X}\neq 0$. We start from the identity (which can be easily proved by the fundamental theorem of calculus),

$$e^{-t\hat{A}}\frac{d}{d\lambda}e^{t\hat{A}} = \int_0^t ds\, e^{-s\hat{A}}\frac{d\hat{A}}{d\lambda}e^{s\hat{A}},$$

where $\hat{A}$ is an arbitrary operator and t is real. By replacing $\hat{A} = \ln\rho$ and $t = 1$, we obtain the following expression for the derivative of the steady-state density matrix (for notational simplicity, we discard the subscript ss of $\hat{\rho}_{\mathrm{ss}}$ and the hat symbol $\hat{}$ for operators in this section),

$$\frac{d}{d\lambda}\rho = \int_0^1 ds\,\rho^{1-s}\frac{d\ln\rho}{d\lambda}\rho^s. \tag{B4}$$

Therefore, Eq. (A1) can be recast into

$$\gamma_{\mu\nu} = -\int_0^\infty dt\int_0^1 ds\,\mathrm{Tr}\big\{e^{-iHt}\rho^{1-s}\partial_\nu(\ln\rho)\rho^s e^{iHt}\partial_\mu H\big\}.$$

Next we apply the equilibrium condition for the steady-state density matrix, $\rho = e^{-\beta H}/Z$ where $Z\equiv\mathrm{Tr}\big\{e^{-\beta H}\big\}$ is the partition function. This condition is equivalent to $\partial_\mu H = \left(-\partial_\mu\ln\rho - \partial_\mu Z/Z\right)/\beta$. Accordingly,

$$\gamma_{\mu\nu} = \frac{1}{\beta}\int_0^\infty dt\int_0^1 ds\,\mathrm{Tr}\big\{e^{-iHt}\rho^{1-s}\partial_\nu(\ln\rho)\rho^s e^{iHt}\partial_\mu(\ln\rho)\big\}. \tag{B5}$$

Notice that another term proportional to $\partial_\mu Z/Z$ vanishes since the integrand becomes $\mathrm{Tr}\{\partial_\nu\rho\} = \partial_\nu\mathrm{Tr}\{\rho\} = 0$ after using Eq. (B4).

Now, in order to see the structure of $\gamma_{\mu\nu}$ more easily, we rewrite the trace in the Lehmann representation, $H|a\rangle = E_a|a\rangle$,

$$\begin{aligned}\gamma_{\mu\nu} =& \sum_{ab}\frac{1}{\beta}\int_0^\infty dt\int_0^1 ds\, e^{-iE_at}\left(\frac{e^{-\beta E_a}}{Z}\right)^{1-s}\langle a|\partial_\nu(\ln\rho)|b\rangle\left(\frac{e^{-\beta E_b}}{Z}\right)^{s}e^{iE_bt}\langle b|\partial_\mu(\ln\rho)|a\rangle\\ =&\frac{1}{\beta}\sum_{ab}\int_0^1 ds\,\rho_a^{1-s}\rho_b^s\langle a|\partial_\nu(\ln\rho)|b\rangle\langle b|\partial_\mu(\ln\rho)|a\rangle\frac{i}{E_b-E_a+i\eta},\end{aligned}$$

where $\rho_a \equiv e^{-\beta E_a}/Z$ (same for ρ_b), and $\eta \to 0^+$. We further split $\gamma_{\mu\nu}$ into the symmetric part and the antisymmetric part, and analyze the symmetric part first,

$$\begin{aligned}\gamma^{\rm S}_{\mu\nu} =&\frac{1}{2}\sum_{ab}\frac{1}{\beta}\int_0^1 ds\,\rho_a^{1-s}\rho_b^s\langle a|\partial_\nu(\ln\rho)|b\rangle\langle b|\partial_\mu(\ln\rho)|a\rangle i\left(\frac{1}{E_b-E_a+i\eta}-\frac{1}{E_b-E_a-i\eta}\right)\\ =&\pi\sum_{ab}\frac{1}{\beta}\int_0^1 ds\,\rho_a^{1-s}\rho_b^s\langle a|\partial_\nu(\ln\rho)|b\rangle\langle b|\partial_\mu(\ln\rho)|a\rangle\delta(E_b-E_a)\\ =&\frac{\pi}{\beta}\sum_{ab}\rho_a\langle a|\partial_\nu(\ln\rho)|b\rangle\langle b|\partial_\mu(\ln\rho)|a\rangle\delta(E_a-E_b).\end{aligned} \tag{B6}$$

Thus,

$$\sum_{\mu\nu}X_\mu\gamma^{\rm S}_{\mu\nu}X_\nu=\frac{\pi}{\beta}\sum_{ab}\rho_a\left|\langle a|\sum_\nu X_\nu\partial_\nu(\ln\rho)|b\rangle\right|^2\delta(E_b-E_a)>0.$$

Second, since the antisymmetric part $\gamma^{\rm A}_{\mu\nu}$ is also real,

$$\sum_{\mu\nu}X_\mu\gamma_{\mu\nu}X_\nu=\sum_{\mu\nu}X_\mu\left(\gamma^{\rm S}_{\mu\nu}+\gamma^{\rm A}_{\mu\nu}\right)X_\nu=\sum_{\mu\nu}X_\mu\gamma^{\rm S}_{\mu\nu}X_\nu>0.$$

Hence, $\gamma_{\mu\nu}$ is positive definite at equilibrium.

C. FLUCTUATION-DISSIPATION THEOREM BASED ON THE QCLE

In this section, we further investigate the fluctuation-dissipation theorem based on the QCLE. Note that the derivation published in the SM of Ref. 2 erroneously divides by zero, but the final result is correct for a real-valued Hamiltonian (as we will now show).

In Ref. 2, a Fokker-Planck equation (or more specifically a Kramer's equation) based on an analysis of the QCLE in the adiabatic theorem was derived along with the corresponding random force $\delta\hat{F}_\mu$ and correlation function $\bar{D}^{\rm S}_{\mu\nu}$.

$$\begin{aligned}\delta\hat{F}_\mu =&-\partial_\mu\hat{H}+{\rm Tr}\Big\{\partial_\mu\hat{H}\hat{\rho}_{\rm ss}\Big\},\\ \bar{D}^{\rm S}_{\mu\nu} =&\frac{1}{2}\int_0^\infty dt\,{\rm Tr}\Big\{e^{i\hat{H}t}\delta\hat{F}_\mu e^{-i\hat{H}t}\left(\delta\hat{F}_\nu\hat{\rho}_{\rm ss}+\hat{\rho}_{\rm ss}\delta\hat{F}_\nu\right)\Big\}.\end{aligned}$$

(We follow the same notation as in Ref. 2, even though $\bar{D}^{\rm S}_{\mu\nu}$ is not symmetric when a complex-valued Hamiltonian is considered here.) Since $\partial_\nu\ln\hat{\rho}_{\rm ss}=\beta\delta\hat{F}_\nu$, we can rewrite Eq. (B5),

$$\gamma_{\mu\nu}=\beta\int_0^\infty dt\int_0^1 ds{\rm Tr}\Big\{(\hat{\rho}_{\rm ss})^{1-s}\,\delta\hat{F}_\nu\,(\hat{\rho}_{\rm ss})^s\,\delta\hat{F}_\mu(t)\Big\},$$

where $\delta\hat{F}_\mu(t)$ is written in Heisenberg picture. We then express both $\gamma_{\mu\nu}$ and $\bar{D}^{\rm S}_{\mu\nu}$ in the Lehmann representation, obtaining

$$\gamma_{\mu\nu} =\beta\sum_{ab}\int_0^\infty dt\int_0^1 ds\,\rho_a^{1-s}\rho_b^s\langle a|\delta\hat{F}_\nu|b\rangle\langle b|\delta\hat{F}_\mu(t)|a\rangle \tag{C7}$$

$$=\beta\sum_{ab}\frac{\rho_b-\rho_a}{\beta(E_a-E_b)}\int_0^\infty dt\,\langle a|\delta\hat{F}_\nu|b\rangle\langle b|\delta\hat{F}_\mu(t)|a\rangle, \tag{C8}$$

$$\bar{D}^{\rm S}_{\mu\nu} =\sum_{ab}\frac{\rho_a+\rho_b}{2}\int_0^\infty dt\,\langle a|\delta\hat{F}_\nu|b\rangle\langle b|\delta\hat{F}_\mu(t)|a\rangle. \tag{C9}$$

At this point, recall that, according to a Kramer's equation, a particle's equation of motion does not depend on the antisymmetric component of the random force correlation function. In other words, if $\mathcal{A}$ is the phase space density of a particle near a surface, the equation of motion for $\mathcal{A}$ satisfies[2]:

$$\partial_t\mathcal{A}=-\sum_\alpha\frac{P_\alpha}{m_\alpha}\partial_\alpha\mathcal{A}-\sum_\alpha F_\alpha\frac{\partial\mathcal{A}}{\partial P_\alpha}+\sum_{\alpha\nu}\gamma_{\alpha\nu}\frac{\partial}{\partial P_\alpha}\left(\frac{P_\nu}{m_\nu}\mathcal{A}\right)+\sum_{\alpha\nu}\bar{D}^{\rm S}_{\alpha\nu}\frac{\partial^2\mathcal{A}}{\partial P_\alpha\partial P_\nu}. \tag{C10}$$

Thus, the physical meaning of the antisymmetric component of $\bar{D}^{\rm S}_{\mu\nu}$ is not clear. Perhaps not surprisingly, then, Equations (C8) and (C9) do not satisfy a "fluctuation-dissipation theorem", $\gamma_{\mu\nu} \neq \beta \bar{D}^{\rm S}_{\mu\nu}$. However, a valid fluctuation-dissipation theorem condition can be established at equilibrium if we consider only the symmetric component of the random force and friction. To do so, we further integrate out the time variable in $\bar{D}^{\rm S}_{\mu\nu}$,

$$\bar{D}^{\rm S}_{\mu\nu} = \sum_{ab} \frac{\rho_a + \rho_b}{2} \frac{i}{E_b - E_a + i\eta} \langle a|\delta\hat{F}_\nu|b\rangle\langle b|\delta\hat{F}_\mu|a\rangle,$$

and then "symmetrize" $\bar{D}^{\rm S}_{\mu\nu}$:

$$\begin{aligned}
&\frac{1}{2}\left(\bar{D}^{\rm S}_{\mu\nu} + \bar{D}^{\rm S}_{\nu\mu}\right) \\
=&\frac{1}{2}\sum_{ab} \frac{\rho_a + \rho_b}{2} \left(\frac{i}{E_b - E_a + i\eta} + \frac{i}{E_a - E_b + i\eta}\right) \langle a|\delta\hat{F}_\nu|b\rangle\langle b|\delta\hat{F}_\mu|a\rangle \\
=&\pi \sum_{ab} \rho_a \langle a|\delta\hat{F}_\nu|b\rangle\langle b|\delta\hat{F}_\mu|a\rangle \delta(E_a - E_b),
\end{aligned}$$

which is equal to $\gamma^{\rm S}_{\mu\nu}/\beta$ when the system is in equilibrium (please compare to Eq. (B6)).

In SM D, we will show that when a real-valued Hamiltonian is considered and the system is in equilibrium, the antisymmetric friction tensor $\gamma^{\rm A}_{\mu\nu}$ vanishes. In this situation, $\gamma_{\mu\nu} = \gamma^{\rm S}_{\mu\nu} = \beta\bar{D}^{\rm S}_{\mu\nu}$.

D. NO ANTISYMMETRIC FRICTION TENSOR $\gamma^{\rm A}_{\mu\nu}$ WHEN THE HAMILTONIAN IS REAL AND THE SYSTEM IS IN EQUILIBRIUM

In this section, we show that the antisymmetric friction $\gamma^{\rm A}_{\mu\nu}$ vanishes when the Hamiltonian is real and the system is in equilibrium (for a non-interacting Hamiltonian). We start from Eq. (A2),

$$\gamma_{\alpha\nu} = -\sum_{kl} \int_{-\infty}^{\infty} \frac{d\epsilon}{2\pi} \langle k|\partial_\alpha \mathcal{H}|l\rangle \frac{1}{\epsilon - \epsilon_l - i\eta} \langle l|\partial_\nu \sigma^{\rm ss}|k\rangle \frac{1}{\epsilon - \epsilon_k + i\eta}, \tag{D11}$$

where $\eta \to 0^+$, and

$$\mathcal{H} = \sum_k \epsilon_k |k\rangle\langle k|.$$

At equilibrium we have

$$\sigma^{\rm ss} = \sum_k P(\epsilon_k)|k\rangle\langle k|,$$

where $P(\epsilon_k) = e^{-\beta\epsilon_k}/\sum_k e^{-\beta\epsilon_k}$ is the Boltzmann distribution. We focus on $\gamma^{\rm A}_{\alpha\nu} \propto \gamma_{\alpha\nu} - \gamma_{\nu\alpha}$. We divide the summation $\sum_{kl}$ in Eq. (D11) into three cases:

$$\sum_{kl} = \sum_{k=l} + \sum_{k\neq l, \epsilon_k \neq \epsilon_l} + \sum_{k\neq l, \epsilon_k = \epsilon_l}. \tag{D12}$$

Also, we utilize the following two identities to replace $\langle l|\partial_\nu\sigma^{\rm ss}|k\rangle$ in Eq. (D11):

$$\partial_\nu \epsilon_k \delta_{lk} = (\epsilon_l - \epsilon_k)\langle l|\partial_\nu|k\rangle + \langle l|\partial_\nu h|k\rangle, \tag{D13}$$

$$\langle l|\partial_\nu\sigma^{\rm ss}|k\rangle = \partial_\nu\epsilon_k \frac{\partial f(\epsilon_k)}{\partial\epsilon_k}\delta_{kl} + \langle l|\partial_\nu|k\rangle\left(f(\epsilon_k) - f(\epsilon_l)\right). \tag{D14}$$

As a result,

$$\begin{aligned}
\gamma^{\rm A}_{\alpha\nu} \propto &\sum_{k\neq l, \epsilon_k\neq\epsilon_l} \int \frac{d\epsilon}{2\pi} \langle k|\partial_\alpha\mathcal{H}|l\rangle \frac{1}{\epsilon - \epsilon_l - i\eta} \left\{-\langle l|\partial_\nu\mathcal{H}|k\rangle \frac{f(\epsilon_k) - f(\epsilon_l)}{\epsilon_l - \epsilon_k}\right\} \frac{1}{\epsilon - \epsilon_k + i\eta} \\
&+ \sum_{k\neq l, \epsilon_k = \epsilon_l} \int \frac{d\epsilon}{2\pi} \{0\} \frac{1}{\epsilon - \epsilon_l - i\eta} \{0\} \frac{1}{\epsilon - \epsilon_k + i\eta} \\
&- (\alpha \leftrightarrow \nu).
\end{aligned} \tag{D15}$$

Note that the diagonal term (the first summation $\sum_{k=l}$ in Eq. (D12)) does not contribute to $\gamma^{\rm A}_{\alpha\nu}$. Similarly, the second line of Eq. (D15) is zero, which is consistent with the assumption we made in deriving the friction tensor Eq. (A1): in order to achieve a well-defined unique steady state $\hat{\rho}_{\rm ss}$ we presume there are no degenerate states.

Next, let's focus on the only contributing summation in Eq. (D15). By using the identities,

$$\frac{c}{2\pi}\int_{-\infty}^{\infty} dy\, e^{icxy} = \delta(x),$$
$$\theta(t_1-t_2) = i\int_{-\infty}^{\infty}\frac{d\omega}{2\pi}\frac{e^{-i\omega(t_1-t_2)}}{\omega+i\eta},$$

we can derive the following expression:

$$\begin{aligned}\int_0^{\infty} dt\, e^{i(E_b-E_a)t} &= \int_{-\infty}^{\infty} dt\,\theta(t)e^{i(E_b-E_a)t} = \int_{-\infty}^{\infty} dt\,\left(i\int_{-\infty}^{\infty}\frac{d\omega}{2\pi}\frac{e^{-i\omega t}}{\omega+i\eta}\right)e^{i(E_a-E_b)t}\\ &= i\int_{-\infty}^{\infty}\frac{d\omega}{2\pi}\frac{1}{\omega+i\eta}\int_{-\infty}^{\infty} dt\, e^{i(E_b-E_a-\omega)t} = \frac{i}{E_b-E_a+i\eta}.\end{aligned} \tag{D16}$$

We then use Eq. (D16) to rewrite the first line in Eq. (D15), obtaining

$$\begin{aligned}&\sum_{k\neq l,\epsilon_k\neq\epsilon_l}\int\frac{d\epsilon}{2\pi}\langle k|\partial_\alpha\mathcal{H}|l\rangle i\int_0^{\infty} dt\, e^{-i(\epsilon-\epsilon_l)t}\left\{-\langle l|\partial_\nu\mathcal{H}|k\rangle\frac{f(\epsilon_k)-f(\epsilon_l)}{\epsilon_l-\epsilon_k}\right\}(-i)\int_0^{\infty} dt'\, e^{i(\epsilon-\epsilon_k)t'}\\ &= \sum_{k\neq l,\epsilon_k\neq\epsilon_l}\int\frac{d\epsilon}{2\pi}\int_0^{\infty} dt\int_0^{\infty} dt'\, e^{i\epsilon(t'-t)}e^{i\epsilon_l t}e^{-i\epsilon_k t'}\langle k|\partial_\alpha\mathcal{H}|l\rangle\left\{-\langle l|\partial_\nu\mathcal{H}|k\rangle\frac{f(\epsilon_k)-f(\epsilon_l)}{\epsilon_l-\epsilon_k}\right\}\\ &= \sum_{k\neq l,\epsilon_k\neq\epsilon_l}\int_0^{\infty} dt\int_0^{\infty} dt'\,\delta(t'-t)e^{i\epsilon_l t}e^{-i\epsilon_k t'}\langle k|\partial_\alpha\mathcal{H}|l\rangle\left\{-\langle l|\partial_\nu\mathcal{H}|k\rangle\frac{f(\epsilon_k)-f(\epsilon_l)}{\epsilon_l-\epsilon_k}\right\}\\ &= \sum_{k\neq l,\epsilon_k\neq\epsilon_l}\int_0^{\infty} dt\, e^{i(\epsilon_l-\epsilon_k)t}\langle k|\partial_\alpha\mathcal{H}|l\rangle\left\{-\langle l|\partial_\nu\mathcal{H}|k\rangle\frac{f(\epsilon_k)-f(\epsilon_l)}{\epsilon_l-\epsilon_k}\right\}\\ &= \sum_{k\neq l,\epsilon_k\neq\epsilon_l}\frac{i}{\epsilon_l-\epsilon_k+i\eta}\langle k|\partial_\alpha\mathcal{H}|l\rangle\left\{-\langle l|\partial_\nu\mathcal{H}|k\rangle\frac{f(\epsilon_k)-f(\epsilon_l)}{\epsilon_l-\epsilon_k}\right\}.\end{aligned} \tag{D17}$$

By using the identity,

$$\frac{1}{\omega\pm i\eta} = \mathcal{P}\frac{1}{\omega}\mp i\pi\delta(\omega),$$

we can recast Eq. (D17) to get

$$\begin{aligned}&i\sum_{k\neq l,\epsilon_k\neq\epsilon_l}\mathcal{P}\frac{1}{\epsilon_l-\epsilon_k}\langle k|\partial_\alpha\mathcal{H}|l\rangle\left\{-\langle l|\partial_\nu\mathcal{H}|k\rangle\frac{f(\epsilon_k)-f(\epsilon_l)}{\epsilon_l-\epsilon_k}\right\}\\ &+\pi\sum_{k\neq l,\epsilon_k\neq\epsilon_l}\delta(\epsilon_l-\epsilon_k)\langle k|\partial_\alpha\mathcal{H}|l\rangle\left\{-\langle l|\partial_\nu\mathcal{H}|k\rangle\frac{f(\epsilon_k)-f(\epsilon_l)}{\epsilon_l-\epsilon_k}\right\}.\end{aligned} \tag{D18}$$

Apparently, the second term is 0 since $\epsilon_k\neq\epsilon_l$. Also, the first term will not contribute if the Hamiltonian is real, since the friction tensor $\gamma_{\mu\nu}$ must be real and so we only need the real part of $\gamma^{\rm A}_{\mu\nu}$. Therefore, we have proven that the antisymmetric friction tensor vanishes when a real Hamiltonian is considered and the system is in equilibrium.

As a side note, Eq. (D15) can be recast in the following form,

$$\gamma^{\rm A}_{\alpha\nu}\propto -\sum_{k\neq l,\epsilon_k\neq\epsilon_l} 2\mathfrak{Im}\left\{d^\alpha_{kl}d^\nu_{lk}\right\}\left[f(\epsilon_k)-f(\epsilon_l)\right],$$

where $d^\alpha_{kl}\equiv\langle k|\partial_\alpha|l\rangle$ is the derivative coupling. As a result, the Lorentz force $-\sum_\nu\gamma^{\rm A}_{\alpha\nu}\dot{R}_\nu$ (which is defined in the main body of the text) becomes the normal Berry force weighted by the Fermi distributions:

$$-\sum_\nu\dot{R}_\nu\gamma^{\rm A}_{\alpha\nu} = 2\mathfrak{Im}\left\{\sum_{k\neq l,\epsilon_k\neq\epsilon_l}\left(\dot{\mathbf{R}}\cdot\mathbf{d}_{lk}\right)d^\alpha_{kl}\right\}\left[f(\epsilon_k)-f(\epsilon_l)\right].$$

E. SCHEMATIC PICTURE OF THE MOLECULAR JUNCTION HAMILTONIAN (EQUILIBRIUM CASE)

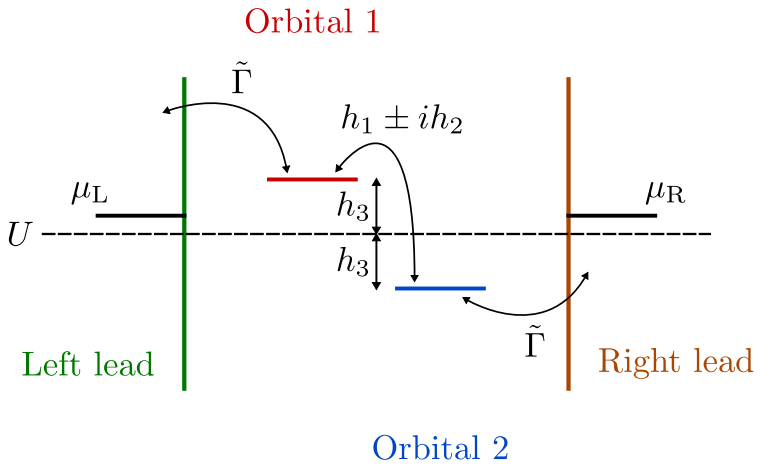


FIG. E1. A schematic picture of the molecular junction Hamiltonian used in the main body of the text. Here we plot the equilibrium case where $\mu_{\rm L} = \mu_{\rm R}$.

F. DERIVING EQUATIONS (3)-(5)

Here we provide a few details as far as deriving Eqs. (3)-(5). Under the approximations made in the main text, the retarded Green's function is

$$G^{\rm R} = \frac{1}{\epsilon - h^{\rm s} - \Sigma^{\rm R}} = \frac{1}{\tilde{\epsilon} - \mathbf{h}\cdot\boldsymbol{\sigma}} = \frac{1}{\tilde{\epsilon}^2 - h^2}\left(\tilde{\epsilon} + \mathbf{h}\cdot\boldsymbol{\sigma}\right),$$

As a result, the lesser Green's function in Eq. (2) can be calculated,

$$G^{<} = G^{\rm R}\Sigma^{<}G^{\rm A} = i\tilde{\Gamma}\left|\frac{1}{\tilde{\epsilon}^2 - h^2}\right|^2 \left(\kappa_0 + \boldsymbol{\kappa}\cdot\boldsymbol{\sigma}\right),$$

where $G^{\rm A} = \left(G^{\rm R}\right)^{\dagger}$.

We then calculate the overall trace in Eq. (2) (recall that $\partial_\epsilon G^{\rm R} = -G^{\rm R}G^{\rm R}$),

$$\begin{aligned}
&C\,{\rm Tr}\left\{\partial_\mu \mathbf{h}\cdot\boldsymbol{\sigma}\left(\tilde{\epsilon}^2 + h^2 + 2\tilde{\epsilon}\mathbf{h}\cdot\boldsymbol{\sigma}\right)\partial_\nu \mathbf{h}\cdot\boldsymbol{\sigma}\left(\kappa_0 + \boldsymbol{\kappa}\cdot\boldsymbol{\sigma}\right)\right\}\\
=&2C\Big\{2\tilde{\epsilon}\left(\partial_\mu\mathbf{h}\cdot\mathbf{h}\right)\left(\partial_\nu\mathbf{h}\cdot\boldsymbol{\kappa}\right) + \left(\tilde{\epsilon}^2 + h^2\right)\kappa_0\partial_\mu\mathbf{h}\cdot\partial_\nu\mathbf{h}\\
&+ i\left(\tilde{\epsilon}^2 + h^2\right)\partial_\mu\mathbf{h}\cdot\left(\partial_\nu\mathbf{h}\times\boldsymbol{\kappa}\right) + i2\tilde{\epsilon}\kappa_0\left(\partial_\mu\mathbf{h}\times\mathbf{h}\right)\cdot\partial_\nu\mathbf{h}\\
&- 2\tilde{\epsilon}\left(\partial_\mu\mathbf{h}\times\mathbf{h}\right)\cdot\left(\partial_\nu\mathbf{h}\times\boldsymbol{\kappa}\right)\Big\},
\end{aligned}$$

In order to calculate the friction tensor, we only need to consider the real part of the trace above, resulting in the final expression of the friction tensor in Eqs. (3)-(5).

G. $h^{\rm s}$ WITH A CONICAL INTERSECTION (EQUILIBRIUM)

In this section, we prove that the antisymmetric friction tensor γ^A_{xy} vanishes when a typical conical intersection (with only linear dependence on the nuclear coordinates) is considered. We then model a simple $E\otimes\epsilon$ Jahn-Teller system in the presence of spin-orbit coupling and a nuclear bath to demonstrate that no significant enhancement of the relative strength of the antisymmetric friction tensor arises from the presence of a conical intersection (which does

provide infinite derivative couplings for an isolated system). To prove these points, assume that a conical intersection is located at $(0,0)$. The most general second order Hamiltonian is

$$\begin{aligned}\mathbf{h}^{\mathrm{s}} &= \mathbf{h}(x,y)\cdot\boldsymbol{\sigma},\\ \mathbf{h}(x,y) &= \mathbf{P}x^2+\mathbf{Q}xy+\mathbf{R}y^2+\mathbf{S}x+\mathbf{T}y,\end{aligned}$$

where $\mathbf{P}$, $\mathbf{Q}$, $\mathbf{R}$, $\mathbf{S}$ and $\mathbf{T}$ are constant vectors. If only two of these constant vectors are nonzero, the antisymmetric friction tensor $\gamma^{\mathrm{A}}_{\mu\nu}$ (which depends on $\mathbf{h}\cdot(\partial_\mu\mathbf{h}\times\partial_\nu\mathbf{h})$) must vanish. This fact indicates that, for a typical conical intersection with a consideration of only linear vibronic terms (only $\mathbf{S}$ and $\mathbf{T}$ are nonzero), there is no antisymmetric friction tensor. Moreover, when there are no linear terms (only $\mathbf{P}$, $\mathbf{Q}$ and $\mathbf{R}$ are nonzero as in a Renner-Teller intersection[50]), $\gamma^{\mathrm{A}}_{\mu\nu}$ must still disappear.

Finally, in order to derive a nonzero $\gamma^{\mathrm{A}}_{\mu\nu}$, we must include a linear complex coupling on top of a second order real-valued $E\otimes\epsilon$ Jahn–Teller system,

$$\mathbf{h}^1=\begin{pmatrix}y^2-x^2 & 2xy\\ 2xy & x^2-y^2\end{pmatrix}+A\begin{pmatrix}-y & x\\ x & y\end{pmatrix}+B\begin{pmatrix}0 & -iy\\ iy & 0\end{pmatrix},$$

This Hamiltonian can be experimentally realized as a regular triangular molecule with two degenerate electronic states interacting with a doublet of vibrational states (up to quadratic order) with a spin-orbit coupling between the p_x and p_y orbitals included.

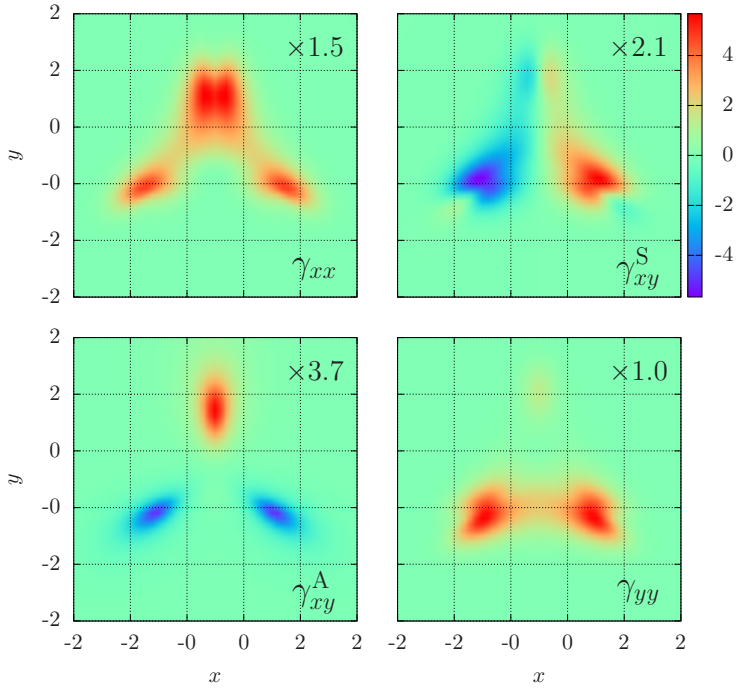


FIG. G2. Friction tensor calculation results near a conical intersection: γ_{xx} (top left), γ^{S}_{xy} (top right), γ^{A}_{xy} (bottom left) and γ_{yy} (bottom right). Parameters: $\tilde{\Gamma}=1$, $\mu_{\mathrm{R}}=\mu_{\mathrm{L}}=0$, $\beta=2$, $A=1$, $B=0.5$. Note that no enhancement of the relative strength of the antisymmetric pseudomagnetic field is caused by a conical intersection. Also, near the conical intersection where the second order vibronic terms can be ignored, γ^{A}_{xy} vanishes.

Figure G2 plots the corresponding friction tensor results, and the ratio $\left|\gamma^{\mathrm{S}}_{yy}/\gamma\right|$. After scanning a reasonable set of parameters, we have never, in practice, been able to find a Hamiltonian where this ratio is more than 25% in the vicinity of the origin. Thus, we do not observe any enhancement of the relative strength of an antisymmetric pseudomagnetic field as caused by a conical intersection. In other words, exactly around a conical intersection, the nuclear dynamics is dominated by dissipation.

H. FRICTION TENSOR AS A FUNCTION OF INVERSE TEMPERATURE β

Next, we investigate the effect of temperature on the friction tensor. Note that, according to Eq. (6) and (7), the friction tensor in Eq. (3) can be represented as $\gamma_{\mu\nu} = \int d\epsilon\,(F^{\rm S}_{\mu\nu} + F^{\rm A}_{\mu\nu})f$. Here $F^{\rm S}_{\mu\nu}$ and $F^{\rm A}_{\mu\nu}$ are the integrands of Eqs. (4) and (5) respectively (excluding the Fermi-Dirac distribution f), namely

$$\begin{aligned} F^{\rm S}_{\mu\nu} =& \frac{1}{\pi}\Big\{ -4\epsilon\mathfrak{Re}\left\{C\tilde{\epsilon}\right\}(\partial_\mu \mathbf{h}\cdot\partial_\nu\mathbf{h})(\mathbf{h}\cdot\mathbf{h}) \\ &+4\epsilon\mathfrak{Re}\left\{C\tilde{\epsilon}\right\}(\partial_\mu \mathbf{h}\cdot\mathbf{h})(\mathbf{h}\cdot\partial_\nu\mathbf{h}) \\ &+4\epsilon\mathfrak{Re}\left\{C\tilde{\epsilon}\right\}(\partial_\mu \mathbf{h}\cdot\mathbf{h})(\partial_\nu\mathbf{h}\cdot\mathbf{h}) \\ &+\left(\epsilon^2+h^2+\frac{\Gamma^2}{4}\right)\mathfrak{Re}\left\{C\left(\tilde{\epsilon}^2+h^2\right)\right\}\partial_\mu\mathbf{h}\cdot\partial_\nu\mathbf{h}\Big\} \end{aligned} \tag{H19}$$

$$\begin{aligned} F^{\rm A}_{\mu\nu} =& \frac{1}{\pi}\Big\{ -2\epsilon\mathfrak{Im}\left\{C\left(\tilde{\epsilon}^2+h^2\right)\right\}\partial_\mu\mathbf{h}\cdot(\partial_\nu\mathbf{h}\times\mathbf{h}) \\ &-2\left(\epsilon^2+h^2+\frac{\Gamma^2}{4}\right)\mathfrak{Im}\left\{C\tilde{\epsilon}\right\}(\partial_\mu\mathbf{h}\times\mathbf{h})\cdot\partial_\nu\mathbf{h}\Big\} \end{aligned} \tag{H20}$$

These integrands contain not only the effect of broadening from the metal (recall that $G^< = -i2f\mathfrak{Im}G^{\rm R}$), but also the derivatives of $h^{\rm s}$ as a function of nuclear coordinates (μ, ν) plus the partial derivative $\partial_\epsilon G^{\rm R}$. Since the temperature appears only in the Fermi-Dirac distribution, changing β effectively controls the overlap between $F^{\rm S}$ and f (and between $F^{\rm A}$ and f). This analysis can lead to the different orders of magnitude for the symmetric and antisymmetric friction tensors. For instance, as shown in Fig 1 of the main text, for the case $\beta = 2$, the antisymmetric tensor is much larger than the symmetric tensor — and this becomes only stronger at even lower temperatures. By comparison, in Fig. H3 we show the contour plots at a higher temperature $\beta = 1$, where the antisymmetric friction tensor is now of the same order of magnitude as the symmetric friction tensor. For a plot of one numerical example of $F(\epsilon)$, see Figs. J14 below.

As a side note, beyond temperature effects, we mention that one could also utilize the chemical potential μ to control $\gamma^{\rm S}$ and $\gamma^{\rm A}$. For instance, since $F^{\rm S}$ and $F^{\rm A}$ are both odd functions of ϵ, when the chemical potential is high or low enough, both $\gamma^{\rm S}$ and $\gamma^{\rm A}$ disappear.

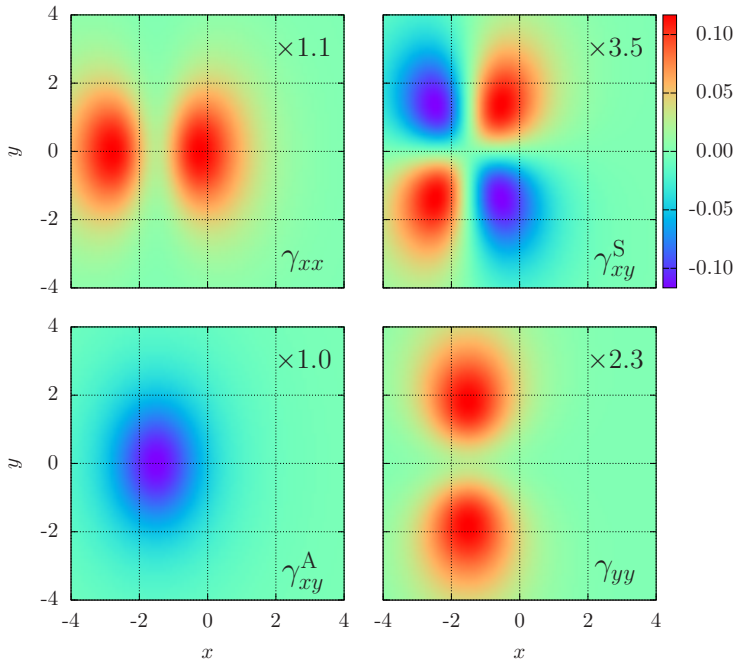


FIG. H3. Friction tensor calculation results: γ_{xx} (top left), $\gamma^{\rm S}_{xy}$ (top right), $\gamma^{\rm A}_{xy}$ (bottom left) and γ_{yy} (bottom right). Parameters: $\tilde{\Gamma} = 1$, $\mu_{\rm R} = \mu_{\rm L} = 0$, $\beta = 1$, $A = 1$, $B = 1$, $\Delta = 3$. Note that we have raised the temperature relative to Fig. 1 in the main text of the letter. We find that the relative strength of the antisymmetric friction tensor $\gamma^{\rm A}_{xy}$ has decreased, though $\gamma^{\rm A}_{xy}$ and $\gamma^{\rm S}$ are still the same order of magnitude.

I. FRICTION TENSOR AS A FUNCTION OF METAL-MOLECULE COUPLING $\tilde{\Gamma}$

For molecules in the gas phase, it is fairly standard to ascertain the size of a Berry force from the relevant derivative couplings[36]. In this manuscript, however, our goal has been to report the size of the Berry force in a condensed environment. Thus, for completeness, in Figs. I4 and I5, we plot the friction tensor as a function of $\tilde{\Gamma}$, which represents coupling of the molecule to the metal. In Fig. I4, we increase $\tilde{\Gamma}$ relative to Fig. 1 in the main text of the letter. We find that the relative strength of the antisymmetric friction tensor γ^{A}_{xy} is effectively unchanged. Furthermore, in general, when $\tilde{\Gamma}$ gets very large, both the antisymmetric and symmetric components of the friction tensor decrease, as shown in Fig. I5.

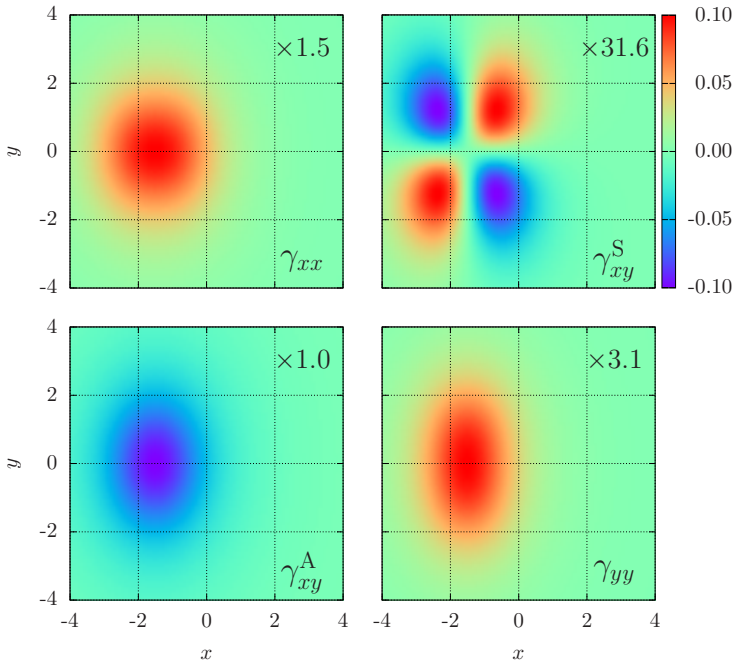


FIG. I4. Friction tensor calculation results as a comparison of different $\tilde{\Gamma}$'s: γ_{xx} (top left), γ^{S}_{xy} (top right), γ^{A}_{xy} (bottom left) and γ_{yy} (bottom right). Parameters: $\tilde{\Gamma} = 3$, $\mu_{\mathrm{R}} = \mu_{\mathrm{L}} = 0$, $\beta = 2$, $A = 1$, $B = 1$, $\Delta = 3$. Note that, as $\tilde{\Gamma}$ increases relative to Fig. 1 in the main text of the letter, the relative strength of the antisymmetric friction tensor γ^{A}_{xy} is effectively unchanged.

J. ONE PROPOSED EXPERIMENTAL REALIZATION: A DIPHENYLMETHANE JUNCTION

In this section, we would like to show how the theory above can be applied within a realistic calculation of a molecule. We focus on the diphenylmethane (which can be easily prepared by a Friedel–Crafts reaction[51]). We imagine a scenario whereby the molecule is placed in a junction between gold electrodes, and for our *ab initio* simulations below, we replace two hydrogen atoms by two gold atoms. As shown in Fig. J6 (a), the optimized geometry has nearly a C_2 symmetry. We perform DFT calculations with the B3LYP exchange functional, LANL2DZ basis and LANL2DZ effective core potential. Among the orbital energies, the LUMO (-0.0874 a.u.) and LUMO+1 (-0.0853 a.u.) are well separated from all other orbitals (HOMO: -0.2333 a.u., LUMO+2: -0.0222 a.u.), which allows us to consider the single-particle Hamiltonian with explicitly two orbitals as described in the main body of the text. Experimentally these two orbitals can be probed by tuning the chemical potential of the nearby electrodes.

Next, in order to apply the friction model constructed in the main body of the text, we further apply a normal mode analysis to isolate the low frequency modes of the molecule. Obviously, diphenylmethane has $3 \times 25 - 6 = 69$ normal modes, and the friction tensor is a large matrix. That being said, our goal here is to show that the antisymmetric component can be crucial, and to that end, it will suffice to focus on only a handful of normal modes that are thermally populated at reasonable temperatures. We will consider the normal mode of lowest frequency plotted in Fig. J7 which has energy $17.3\,\mathrm{cm}^{-1}$. Over this mode, we scan the orbital energies of the LUMO and LUMO+1, and follow the standard Boys localization procedure [52] to obtain two diabats and a corresponding diabatic coupling. In Fig. J8, we plot the orbital energies of LUMO (blue), LUMO+1 (red), the two localized diabat energies (black cross)

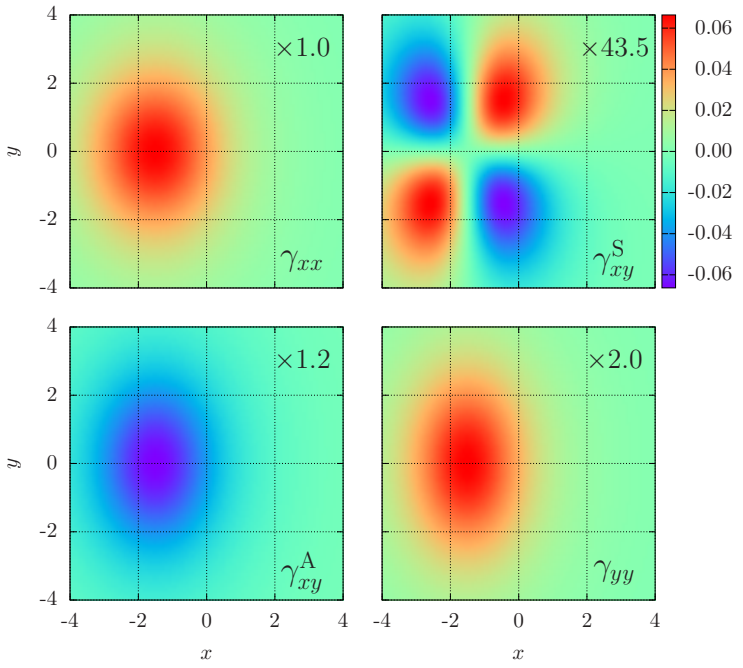


FIG. I5. Friction tensor calculation results as a comparison of different $\tilde{\Gamma}$'s: γ_{xx} (top left), γ^{S}_{xy} (top right), γ^{A}_{xy} (bottom left) and γ_{yy} (bottom right). Parameters: $\tilde{\Gamma} = 5$, $\mu_{\mathrm{R}} = \mu_{\mathrm{L}} = 0$, $\beta = 2$, $A = 1$, $B = 1$, $\Delta = 3$. Note that when $\tilde{\Gamma}$ gets very large, both the antisymmetric and symmetric components of the friction tensor decrease in magnitude.

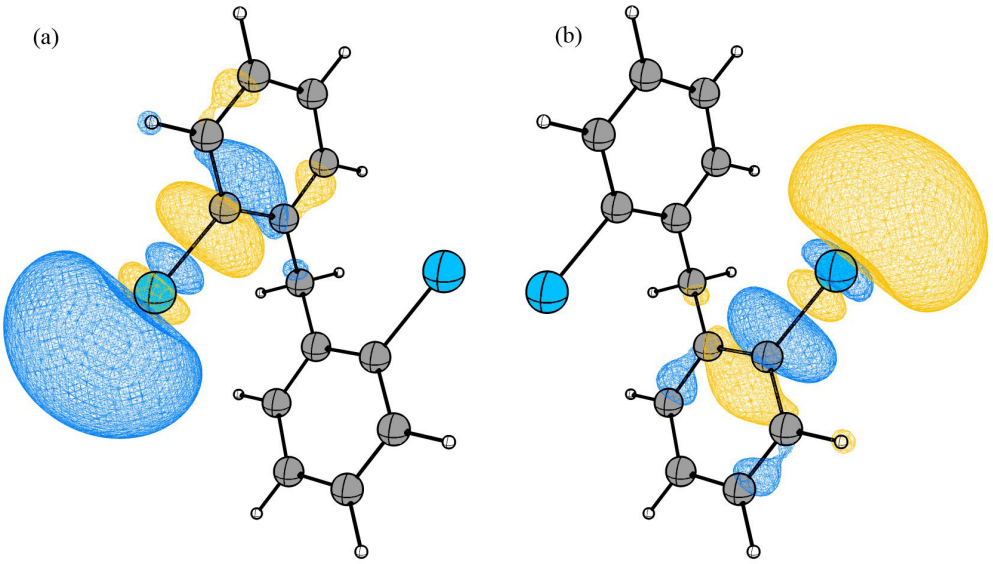


FIG. J6. Optimized geometry of diphenylmethane with two hydrogen atoms (white) replaced by two gold atoms (blue), which heuristically represent two gold clusters. We map the two localized orbitals in (a) and (b) to the two diabats used to construct the system Hamiltonian $\mathbf{h}^{\mathrm{s}}$ in the main body of the text.

and the corresponding diabatic coupling; the diabatic orbital information will be used in constructing the system Hamiltonian $\mathbf{h}^{\mathrm{s}}$ in the main body of the text. Notice that, as shown in Fig. J6, the two diabats 1 and 2 are localized near the two different gold atoms, which justifies the assumption that the hybridization function (Γ_{mn}) be diagonal; $\Gamma_{12} = 0$.

The two diabats and the diabatic coupling in Fig. J8 form the system Hamiltonian $\mathbf{h}^{\mathrm{s}}$ in the main body of the text. The diagonal terms of $\mathbf{h}^{\mathrm{s}}$ can be divided into symmetric and antisymmetric parts, $h_0 I$ and $h_3\sigma_3$ respectively, and we disregard the symmetric part since it does not affect the friction tensor. The antisymmetric term is shown in

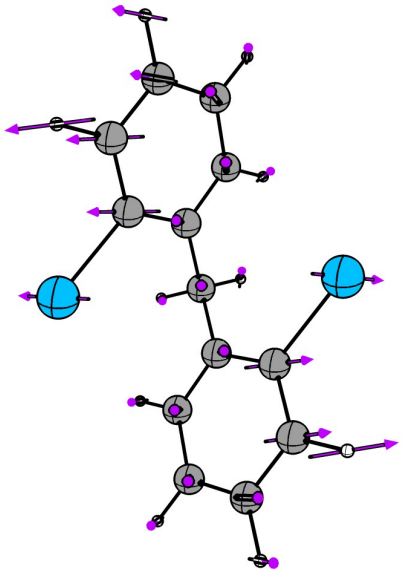


FIG. J7. Normal mode of the diphenylmethane with the lowest frequency.

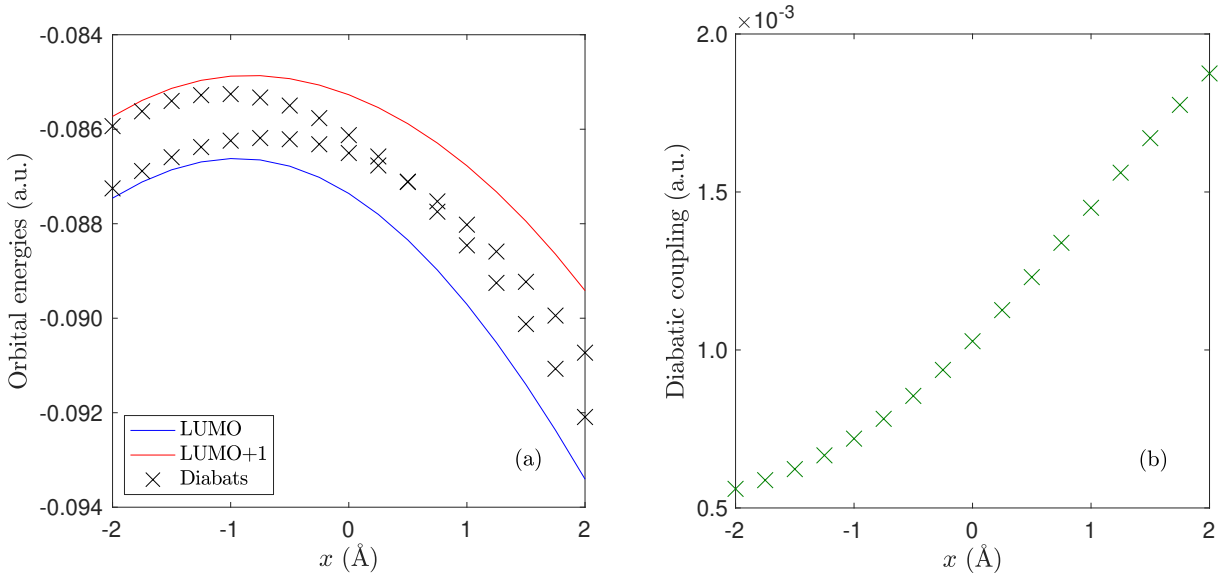


FIG. J8. (a) Orbital energies of LUMO (blue) and LUMO+1 (red) along the lowest normal mode. The two diabats (black cross) are obtained through standard Boys localization, and (b) is the corresponding diabatic coupling.

Fig. J9. As one can observe in Fig. J8 (b) and Fig. J9, the diabatic coupling and h_3 are not exactly linear functions. Nevertheless, for simplicity and in order to be consistent with the main text, we will make a linear approximation so as to estimate the order of magnitude of the parameters in our model. The linear functions for h_3 and the diabatic coupling are fit to $\lambda x + \Delta$ and $Ax + C$ respectively where $\lambda = 3.44 \times 10^{-4}$, $\Delta = -1.13 \times 10^{-4}$, $A = 3.44 \times 10^{-4}$ and $C = 1.11 \times 10^{-3}$ (all in the a.u.). Note that the room temperature is $k_{\mathrm{B}}T = 25.7\,\mathrm{meV} = 9.45 \times 10^{-4}\,\mathrm{a.u.}$, and low temperature experiments can be easily done nowadays. We will estimate $\tilde{\Gamma}$ according to Refs. 53–55, assuming the value ranges from $1 - 100\,\mathrm{meV}$. (In Ref. 53, the authors set the spin-orbit interaction to be one order smaller than the diabatic coupling).

At this point, the only unknown in our model is the strength of the spin-orbit coupling. Unfortunately, estimating matrix elements rigorously is very demanding and convergence is not easy to achieve: are fully relativistic two-component simulations necessary (or can we use perturbation theory on top of spin-restricted spin-collinear DFT)? Gold atoms introduce a great deal of spin-orbit coupling, but how many gold atoms must be included in a cluster for

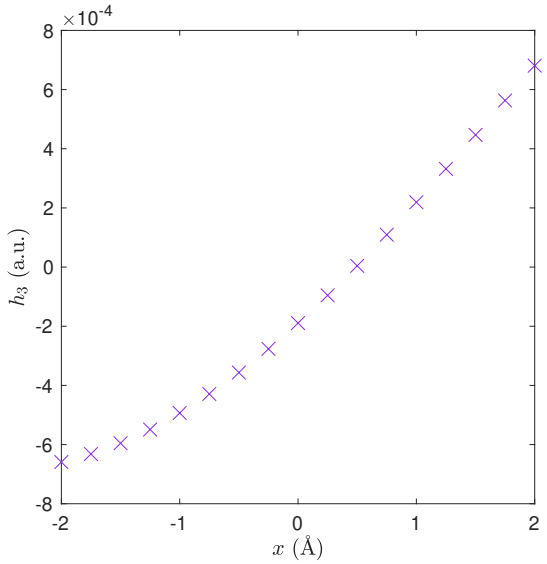


FIG. J9. The σ_3 component, h_3, used for the friction tensor calculations.

convergence? Answering these questions remains a hot topic within the field[56]. Note also that calculations become much more demanding with increasing system size, such that implementing a high level code make sampling nuclear configurations quite expensive. For all of these reasons, we will simply follow Refs. 53–55 and fit the spin-orbit interaction to be of the form by $By + C'$ where the parameters are chosen as as either the same order of magnitude as the diabatic coupling ($B = A$, $C' = C$) or 5% times smaller than the diabatic coupling ($B = 0.05A$ and $C' = 0.05C$) (which is smaller than any estimates in Refs. 53–55).

In the following, we provide some representative results. In Fig. J10, we show contour plots for the friction tensor with $\tilde{\Gamma} = 10\,\text{meV}$ and $B = A$ under room temperature. The antisymmetric friction tensor is comparable to the symmetric friction tensors and this phenomenon is still robust for larger $\tilde{\Gamma} = 100\,\text{meV}$. Also notice that the effective regions for the two kinds of friction tensors are quite different so that the nuclear motion will be strongly affected by the pseudo magnetic field.

Next, we address the common situation whereby the spin-orbit coupling matrix elements are small (i.e. much smaller than the diabatic couplings). In Fig. J11, we show contour plots for the friction tensor with $B = 0.1A$ (still under room temperature and $\tilde{\Gamma} = 30\,\text{meV}$). Observe that the antisymmetric friction tensor becomes one order smaller than the symmetric ones. Nevertheless, when the temperature is decreased, γ^{A}_{xy} gets relatively larger as shown in Fig. J12. In fact, for this case, changing temperature can make γ^{A}_{xy} dominant even when the spin-orbit interaction is extremely small ($B = 0.05A$) (especially if we reduce $\tilde{\Gamma}$) as shown in Fig. J13. In Fig. J14, in order to further explore the effect of temperature on this system, we plot the integrands F^{S}_{xx} and F^{A}_{xy} (as defined in Sec. H) for one specific geometry. As mentioned in Sec. H, both F^{S}_{xx} and F^{A}_{xy} are antisymmetric functions, so that when we integrate $\int d\epsilon\,(F^{\text{S}}_{\mu\nu} + F^{\text{A}}_{\mu\nu})f$ so as to evaluate the friction tensor, we require only the antisymmetric part of the Fermi distribution, f^{A}, as shown in Fig. J14. For this one geometry, it is clear that, as the temperature is lowered, the symmetric friction tensor becomes smaller due to a cancellation between positive and negative integral areas, and the antisymmetric friction tensor becomes larger. The generality of these findings (and surprising temperature effects on friction) will need to be addressed and investigated in more detail for many more molecules and geometries in the future.

Lastly, we investigate how the chemical potential $\mu_L = \mu_R = \mu$ affects the friction tensors. In Fig. J15, we plot both symmetric and antisymmetric friction tensors as a function of the chemical potential μ. When μ is away from zero, the symmetric friction tensor becomes larger and the antisymmetric friction tensor becomes smaller. Both friction tensors approach zero when $\mu \to \pm\infty$, which has been discussed in SM H.

In summary, we have demonstrated that the antisymmetric friction tensor γ^{A}_{xy} can be as large and sometimes larger than the symmetric friction tensor for a real system, even when the spin-orbit interaction is small (at least at low temperatures). Therefore, for the case of a molecule on a metal surface, one must expect that the contribution of this tensor component cannot be ignored when we consider the rate of vibrational relaxation. As far as understanding the implications for a molecule between two metals (as in the diphenylmethane example here), the possibility that such an antisymmetric force will generate a spin-current is also an intriguing possibility, one that will be investigated in a

future publication as well.

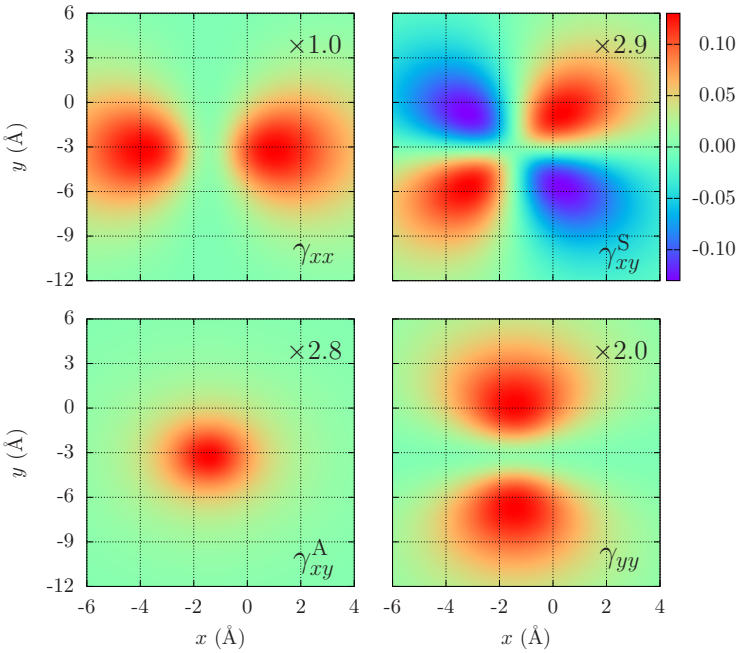


FIG. J10. Friction tensor calculation results: γ_{xx} (top left), γ^{S}_{xy} (top right), γ^{A}_{xy} (bottom left) and γ_{yy} (bottom right). Parameters: $\tilde{\Gamma} = 10\,\mathrm{meV}$ and $B = A$ under room temperature.

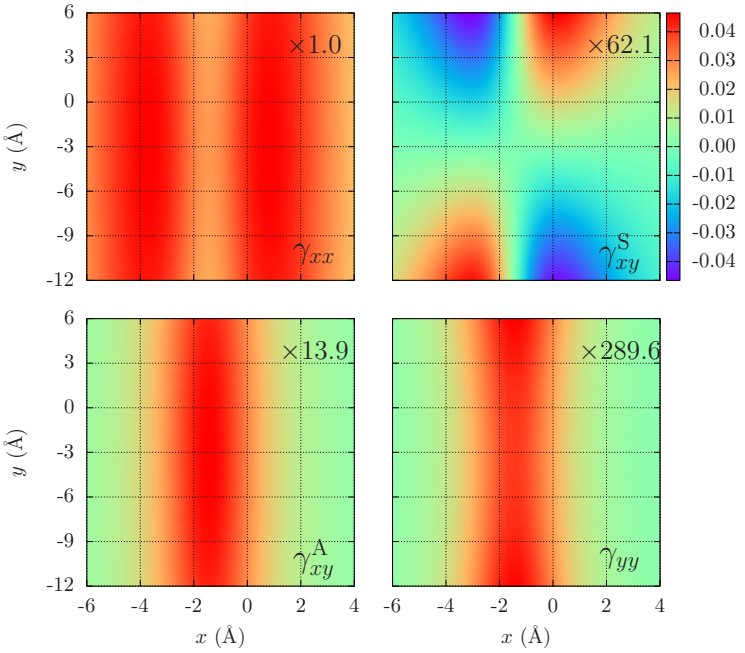


FIG. J11. Friction tensor calculation results: γ_{xx} (top left), γ^{S}_{xy} (top right), γ^{A}_{xy} (bottom left) and γ_{yy} (bottom right). Parameters: $\tilde{\Gamma} = 30\,\mathrm{meV}$ and $B = 0.1A$ under room temperature.

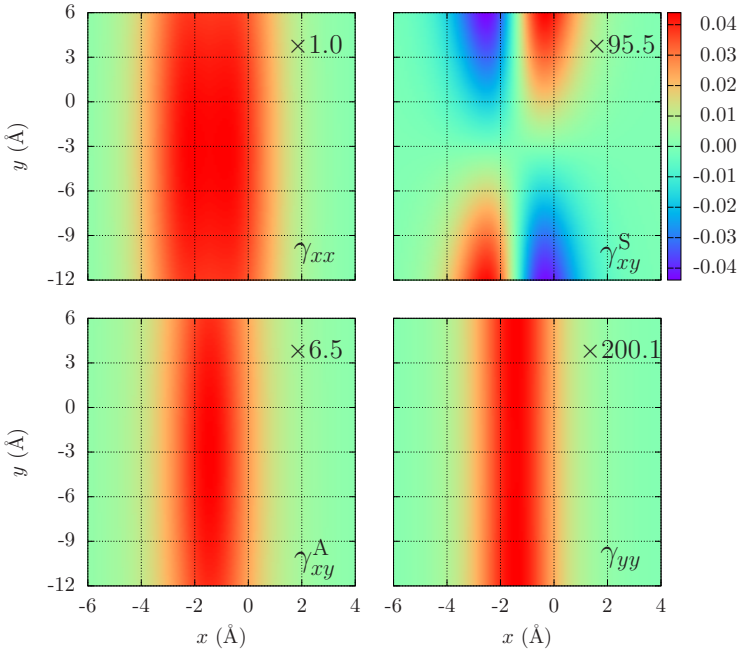


FIG. J12. Friction tensor calculation results: γ_{xx} (top left), γ^{S}_{xy} (top right), γ^{A}_{xy} (bottom left) and γ_{yy} (bottom right). Parameters: $\tilde{\Gamma} = 30\,\mathrm{meV}$, $k_{\mathrm{B}}T = 8.6\,\mathrm{meV}$ and $B = 0.1A$.

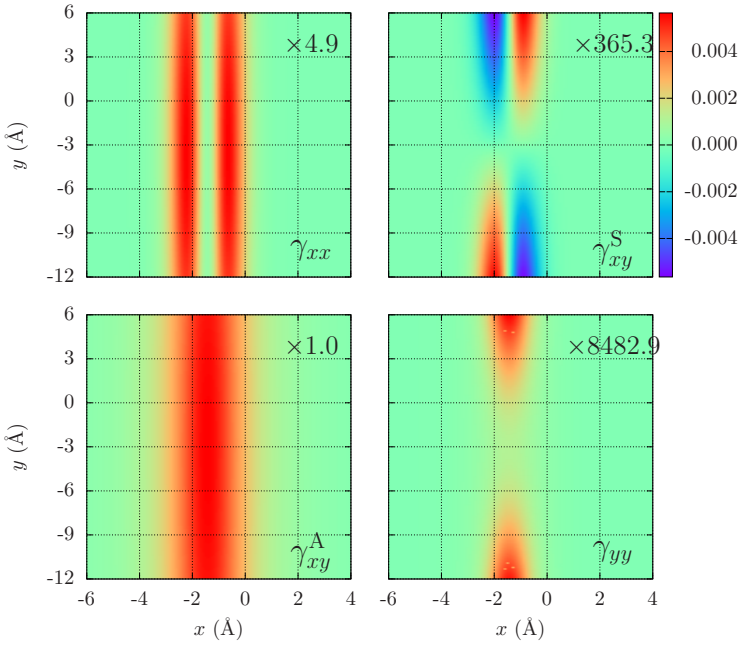


FIG. J13. Friction tensor calculation results: γ_{xx} (top left), γ^{S}_{xy} (top right), γ^{A}_{xy} (bottom left) and γ_{yy} (bottom right). Parameters: $\tilde{\Gamma} = 1\,\mathrm{meV}$, $k_{\mathrm{B}}T = 2.6\,\mathrm{meV}$ and $B = 0.05A$.

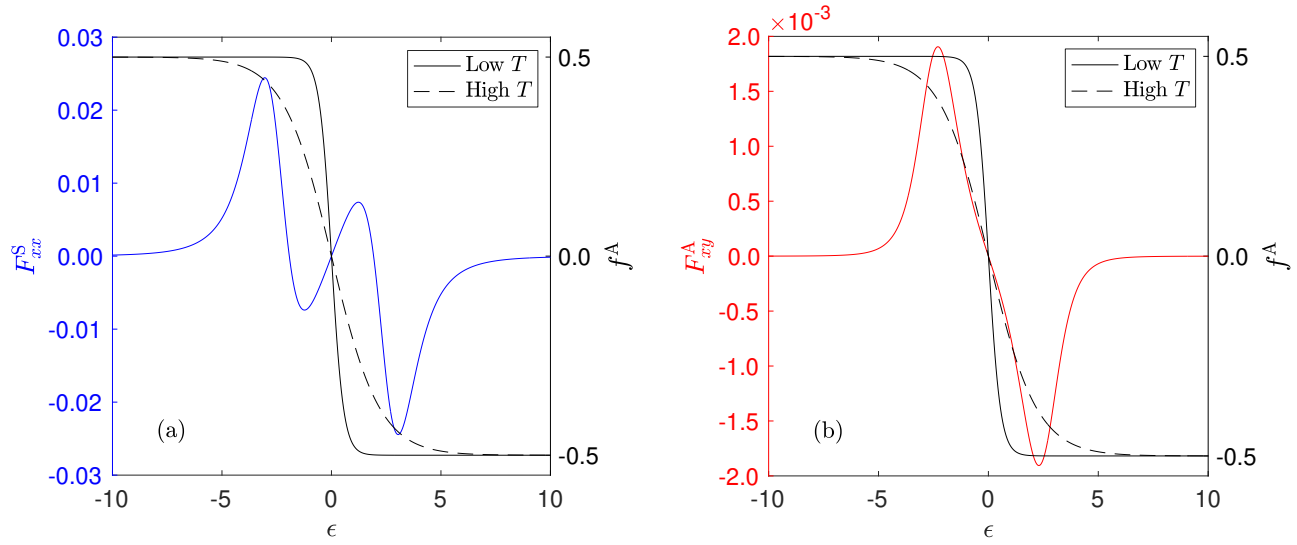


FIG. J14. Integrands for the diphenylmethane at one geometry. Blue and red lines represent the integrands F^{S}_{xx} and F^{A}_{xy} respectively as defined in Sec. H. Black lines (solid for low T, dash for high T) represent the antisymmetrized Fermi distributions f^{A}. As the temperature is lower, the symmetric friction tensor becomes smaller and the antisymmetric friction tensor becomes larger. Parameters: $x = -1.4$, $y = -3.2$, $\tilde{\Gamma} = 30\,\mathrm{meV}$, $B = 0.05A$.

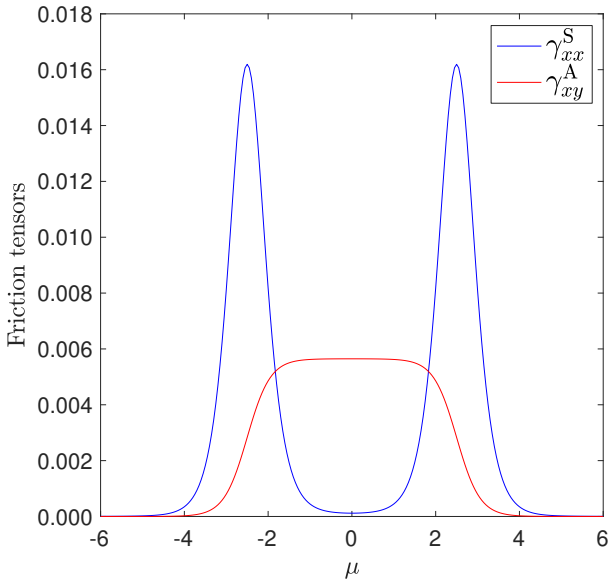


FIG. J15. Friction tensors as a function of μ for the diphenylmethane at one geometry. Blue and red lines represent γ^{S}_{xx} and γ^{A}_{xy} respectively. As the chemical potential is away from zero, the symmetric friction tensor becomes larger and the antisymmetric friction tensor becomes smaller. Both friction tensors approach zero when $\mu \to \pm\infty$. Parameters: $x = -1.4$, $y = -3.2$, $\tilde{\Gamma} = 1\,\mathrm{meV}$, $k_{\mathrm{B}}T = 2.6\,\mathrm{meV}$, $B = 0.05A$.